THE EFFECT OF THE REYNOLDS NUMBER ON THE WING VORTICES

Kyösti Kaarlonen[#], Seppo Laine[#], Esa Salminen[§], and Timo Siikonen[§]
Helsinki University of Technology, P.O. Box 4100, FIN-02015 HUT, Finland

Keywords: *Delta wing, vortex system, Reynolds number*

Abstract

In this work, the flow field around a delta-wing configuration with rounded leading edges, ELAC-1, was studied using computational fluid dynamics (CFD). Wind tunnel experiments have shown that the vortex system of the ELAC-1 configuration depends on the Reynolds number. In the experiments, the Reynolds number range was from 2 to 40 million. The purpose of this study was to examine the Reynolds number effect by using a Navier-Stokes flow solver with two advanced turbulence models, an explicit algebraic Reynolds stress model (EARSM) and a k-ω SST model.

In the computations, four different Reynolds numbers from $3.7x10^6$ to $39x10^6$ were used at an angle of attack of 12°. In addition, some cases with angles of attack of 5, 12.7, 16, 20, 21 and 24° were also studied. The boundary layer was assumed either fully turbulent or fully laminar or partially laminar.

According to the calculations, the Reynolds number has a minor effect on the flow field if the separation line near the leading edge does not move with the Reynolds number. However, if the transition position moves with the change of the Reynolds number, the separation line is possibly replaced thus affecting a change in the flow field. The EARS model produced physically more correct results than the k-ω SST model.

1 Introduction

The ELAC-1 configuration, representing an aerospace design, consists mainly of a delta wing with an aspect ratio of 1.1, see Fig. 1. The wing has a rounded leading edge, a sweep angle of 75° and stabilizer fins at the wing tips. Low-speed wind tunnel experiments for the ELAC-1 (Elliptic Aerodynamic Configuration) have shown that the Reynolds number affects the vortex system of the wing and, therefore, the pressure distribution on the upper surface [1, 2]. In the experiments, the Reynolds number based on the root chord c was varied from $2x10^6$ to $39.7x10^6$. The changes in pressure distributions, especially the values of the suction peaks and their positions do not behave monotonically as a function of the Reynolds number.

The aim of the work was to study computationally the effect of the Reynolds number on the vortex system of the ELAC-1 wing to find an explanation for the observed phenomena. The study was carried out by numerically solving the Reynolds-averaged Navier-Stokes equations. In the computations, two different turbulence models were utilized: an explicit algebraic Reynolds stress model (EARSM) [3, 4] and the k-ω SST model [5].

2 Experimental results

According to Ref. [1], a linear relation exists between the lift coefficient and an angle of attack α for α < 8°. As α > 8°, a concentrated vortex system begins to form, causing additional nonlinear lift forces. The location of the primary separation line and also the strength and location of the vortex system depend on the Reynolds number. The boundary layer is laminar on the lower side of the wing at all

---

[#] Laboratory of Aerodynamics
[§] Laboratory of Applied Thermodynamics

tested Reynolds numbers due to accelerated flow. At Reynolds numbers up to $11.9x10^6$, the transition to turbulent flow occurs just above the leading edge. For Reynolds numbers equal to $19.8x10^6$ and higher, the boundary layer becomes turbulent upstream of the leading edge. The flow can then follow the rounded leading edge, and primary separation occurs on the suction side at about 98% of the local semispan.

Figure 2 presents the pressure coefficient distributions at $\alpha = 12^o$ on the wing surface for five different Reynolds numbers. As can be seen, the primary vortex produces a suction peak, but its strength and position vary with the Reynolds number. At $x/c = 0.3$, the position of the suction peak is at $y/s_{local} = 0.75$ for $Re = 7.9x10^6$ and $Re = 11.9x10^6$, and the separation occurs at the leading edge. Here s_{local} denotes the local semi-span. At higher Reynolds numbers, the separation occurs on the upper surface of the wing. The position of the suction peak moves inboard and its strength reduces at $Re= 19.8x10^6$. At still higher Reynolds numbers, the suction peak is again closer to the leading edge but is much lower.

At section $x/c = 0.6$, the suction peak is highest for the lowest Reynolds number, and it reduces drastically at $Re = 11.9x10^6$ to increase again with a further increase of the Reynolds number. Because of a larger leading edge radius at $x/c = 0.6$ compared to that at $x/c = 0.3$, the flow separates on the upper surface side even at the lowest Reynolds number. This can be seen from the suction peak at the leading edge. On the lower surface, the Reynolds number has a very weak effect on the pressure distribution.

Although the pressure distributions differ considerably, the effect of the Reynolds number on the lift is negligible. The effect on drag is noticeable only around $\alpha = 10^o$.

There exists a weak secondary vortex between the primary vortex and the leading edge. Figure 3 depicts the velocity vectors at a cross-section plane, showing the structure and position of the primary and secondary vortex. Although a tertiary vortex is observed, it is so weak that it has no noticeable effect on the pressure distribution.

3 Numerical method and turbulence models

3.1 Flow solver

The numerical approach used in the present work to solve the Reynolds-averaged Navier-Stokes equations for compressible flows is a finite-volume method, and the flow solver is called FINFLO [6]. The code is based on the structured multi-block grid topology. Roe's method is applied with upwind biased second-order differences for the inviscid fluxes and second-order central differencing for the viscous fluxes. The equations are solved by an implicit pseudo-time integration scheme based on DDADI-factorization. A multigrid technique is employed to speed up the convergence. The code is valid for an approximate Mach number range from 0.1 to 5. Many different turbulence models from algebraic mixing-length models up to full differential Reynolds stress closures have been implemented in the FINFLO code.

3.2 Turbulence models

The turbulence model has a decisive role in the accuracy of the calculation. Therefore, it is important to use a model that can operate in vortical flows with reasonable accuracy. The primary approach used in the present study is an explicit algebraic Reynolds stress model. For a comparison, the k-ω SST model was employed. No streamline curvature correction was applied in the turbulence models.

The EARSM is based on the use of a two-equation model, like the k-ω SST model, and on the equation for the stress anisotropy **a.** The stress anisotropy tensor **a** is defined as follows:

$$a_{ij} = \frac{\overline{u_i^{'} u_j^{'}}}{k} - \frac{2}{3}\delta_{ij} \qquad (1)$$

where $u_i^{'}$ is the fluctuating velocity component, k is the kinetic energy of turbulence and δ_{ij} is the Kronecker δ.

A transport equation for the Reynolds stress anisotropy tensor **a** can be derived in a similar way as the transport equation for the Reynolds stress component tensor. In flows

where the anisotropy varies slowly in time and space, the convection and diffusion in the transport equation can be ignored, and the result is an implicit algebraic equation for *a.* For computational reasons, this equation is then employed to yield an explicit algebraic Reynolds stress model [3].

In the numerical solution approach, the equations for the turbulent kinetic energy k and for the specific dissipation ω are coupled with the mean flow equations. The anisotropy tensor is then determined and the Reynolds stresses are calculated. The EARS model requires about 15% more computational time than a linear two-equation model, like the k-ω SST model. The implementation of the EARSM in the FINFLO code is described in Ref. [4]. The calculated results given below are obtained with the EARS model except where otherwise stated.

In areas of laminar boundary layer flow, the laminarity of the boundary layer is maintained by suppressing the production of turbulence in the calculations at wall distance $y^+<500$.

3.3   Computational grid

Only symmetric flow cases (no side slip) were studied and therefore just one half of the wing was calculated. The grid is of the O-O type, and it was divided into 24 blocks for efficient use in a multiprocessor computer. The first grid had 192x96x160 cells in chordwise, normal and spanwise directions, respectively, resulting in 2,949,120 grid cells around half of the wing. The surface grid duplicated for the full body is depicted in Fig. 4. However, this grid turned out to be somewhat too coarse in the primary vortex area, and therefore a denser grid with $192x128x224 = 5,505,024$ cells was employed for the subsequent calculations. The height of the surface cells corresponding to about $y^+ = 1$ is small enough for a good numerical accuracy.

4   Calculated results

4.1   Flow cases studied

In all, 25 different cases were calculated according to Table 1. They were selected to

cover the Reynolds number range of the experiments and low and high angles of attack.

Table 1. Calculated cases.

Reynolds number	α	Transition position	Turbulence model	Remarks
3.7x10⁶	5	fully turbulent	EARSM	Denser grid
	12			
	20	fully turbulent	EARSM	
	24			
5.9x10⁶	21	fully turbulent	EARSM	
7.9x10⁶	12	fully laminar		
		fully turbulent	EARSM	
		fully turbulent	k-ω SST	
		Upper surface 5% local span ¹	EARSM	
		Upper surface 2% local span ¹	EARSM	
		Upper surface 0.3% local span ¹	EARSM	
		fully turbulent	EARSM	Leading edge blowing
		fully turbulent	EARSM	Blowing 2 % of span
		fully turbulent	EARSM	Denser grid
		Upper surface 2% local span ¹	EARSM	Denser grid
	12.7	fully turbulent	EARSM	Denser grid
	16	fully turbulent	EARSM	
19.8x10⁶	12	fully turbulent	EARSM	
			EARSM	Denser grid
			k-ω SST	
39.0x10⁶	12	fully turbulent	EARSM	
			k-ω SST	
			EARSM	Blowing 2 % of span
			EARSM	Denser grid
	16		EARSM	

1) Lower surface laminar

In most cases the flow is assumed to be fully turbulent, but in some cases it is assumed to be laminar on the lower surface and on the upper surface from the leading edge to the 95%, 98% or 99.7% position of the local semispan. Here the laminar flow means that the production of turbulence is suppressed inside the boundary layer, but the flow can become turbulent outside it. This was done to change the position of the primary separation line and to see its effect on the vortex system. Fully turbulent means a case where the boundary layer is turbulent. In addition, one fully laminar case was calculated. Furthermore, fully turbulent cases with leading edge blowing were computed. The blowing was used to affect the primary separation without the use of the laminarization but keeping the flow

fully turbulent. Then it is possible to see the effect of the nature of separation (laminar or turbulent) on the vortex system. The angle of attack varied from 5° to 24°. Typically 10,000 iterations were required to obtain a converged result.

4.2 Dependence on the angle of attack at $Re=3.7x10^6$

To compare the calculations with experiments in situations where the separation is not affected by the Reynolds number, flow at high angles of attack, 20° and 24°, was simulated at $Re = 3.7x10^6$. (At such high angles of attack the separation occurs on the leading edge of the wing.) In these cases, the agreement between the calculated and measured pressure distributions on the upper surface at a spanwise section of $x/c = 0.6$ is excellent, as can been seen in Fig. 5. Both the primary vortex and secondary vortex are well captured. This may indicate that the EARS model is capable of producing accurate results when the separation occurs at the right position.

At a lower angle of attack, $\alpha=12^o$, the agreement between the calculations and experiments is no longer as perfect. The calculations reproduce the height of the suction peak of the primary vortex correctly but its position is too far from the leading edge. Now, according to the calculations, the separation occurs on the wing upper surface and not along the leading edge as at the two higher angles of attack.

4.3 Angle of attack 12°

Figure 6 depicts the measured and calculated pressure distribution on the surface of the wing at the cross-section $x/c = 0.6$ for a fully turbulent case at $\alpha = 12^o$ for $Re = 7.9x10^6$, $19.8x10^6$, and $39x10^6$ ($39.7x10^6$ at experiments). As can be seen, the agreement with the experiments is not very good. The calculations produce qualitatively correctly the primary vortex suction peak, but the position and strength of the peak are not very accurate. According to the calculations, the two lower Reynolds numbers produce almost identical

pressure distributions, whereas the result of the highest Reynolds number gives a weaker suction peak. But in the measured data, the lowest and the highest Reynolds number have almost equal pressure distributions, and the medium Reynolds number has a weaker suction peak. The suction peak of the leading edge is rather well captured. On the lower side of the wing, the computed pressure distributions agree fairly well with the measurements.

Effect of separation position

To test the effect of separation position on the results, cases with partially laminar boundary-layer flow and a fully turbulent case with leading edge blowing was determined. Figure 7 shows the pressure distributions at $Re = 7.9x10^6$ at $x/c = 0.3$. The laminarization of the boundary layer near the leading edge is seen to improve the results, i.e. the suction peak moves towards the measured value. The results of the three partially laminar cases are almost identical with each other. However, the agreement with measurements is not quite satisfactory.

Figure 8 presents the computed position of separation, the axis of the primary vortex and the constant pressure coefficient curve $C_p = -0.5$ for the case $Re = 7.9x10^6$ at $x/c = 0.3$. Here, the results obtained with the EARSM and with the k-ω SST model are shown. The separation occurs in the partially laminar cases much earlier than in the fully turbulent cases. The earlier separation moves the vortex axis towards the leading edge, and the suction area indicated by the curve $C_p = -0.5$ is larger than for the fully turbulent cases. The k-ω SST model gives a later separation than the EARS model, and the position of the vortex axis is closer to the wing surface.

Figure 9 shows the influence of blowing on the pressure distribution at $x/c = 0.3$ and at $Re = 7.9x10^6$. The blowing velocity is 0.5% of the free-stream velocity and is normal to the surface. The blowing region is four cells wide. There are two blowing cases; in the first case, the blowing takes place along the leading edge. In the second case, the blowing region is just upstream of the separation line of the fully

turbulent case, i.e. along the line y/s_{local} = 0.98. As can be seen, the blowing along the leading edge has a similar effect on the flow as the laminarization of the boundary layer near the leading edge. In these cases, the pressure distributions are in agreement. This result indicates that the separation position is an important factor affecting the structure of the vortex and the pressure distribution. Instead, it does not matter whether the boundary layer is laminar or turbulent at separation. If the blowing occurs at the 98% line, the suction peak is weaker than in the case where the blowing occurs along the leading edge.

Effect of turbulence model

The effect of the turbulence model on the results was studied by calculating the flow at α=12° and at Re=7.9$x10^6$, 19.8$x10^6$, and 39$x10^6$ employing the two different turbulence models. As an example, Fig. 10 depicts the intensity of turbulence at a cross-section x/c = 0.3 and at Re=39$x10^6$. The EARS model gives low values of turbulence inside the core area of the primary vortex, which is in agreement with the experiments, whereas the k-ω SST model produces high values of turbulence. As another distinct feature, the location of the vortex axis given by the EARS model is higher than that given by the k-ω SST model. The figure also shows that, in addition to the primary vortex, a secondary vortex and even a tertiary vortex exist. This is in agreement with the experiments where a tertiary vortex has been observed as well.

Effect of grid density

Figure 11 depicts the effect of grid density on the pressure distribution on the wing surface at x/c = 0.3. The denser grid (5.5$x10^6$ cells) produces a sharper suction peak than the coarser grid (2.9$x10^6$ cells) but the discrepancy between the calculations and the experiments does not diminish appreciably. Both grids give almost equal lift and drag values. Therefore it seems that even the coarser grid is dense enough for studying the effect of the Reynolds number on the vortex system.

4.4   Angle of attack 16°

The flow was computed at α = 16° at Reynolds numbers 7.9$x10^6$ and 39.7$x10^6$. The pressure distributions are given in Fig. 12 at cross-sections x/c = 0.3 and 0.6. According to the measurements, the lower Reynolds number gives a higher suction peak at x/c = 0.3 than the higher Reynolds number case, and at x/c = 0.6 the opposite is true. In the calculations, the Reynolds number has a very small effect on the suction peak, and especially at x/c = 0.3 the position of the suction peak is well predicted. In fact, at Re = 39.7$x10^6$ the calculations agree fairly well with the experiments. Both calculations were carried out assuming the boundary layer fully turbulent, since now the primary separation occurs at the leading edge for all Reynolds numbers, both in the experiments and in the calculations.

4.5   Lift and drag

The reference area used in the calculations corresponds in full scale to 1,389 m^2. Calculated lift coefficients at α = 12° were in the range of 0.017 to 0.029 too low compared to the measured values, and the calculated drag coefficients were 2 to 20% too low. At α = 16° the calculated lift coefficients were from 0.03 to 0.045 too low and the drag coefficients from 8 to 18 % too low. This indicates that the strength of the primary vortex in the calculations is weaker than in the experiments.

To study the possible reason for this discrepancy, one case was calculated at 12.7° for Re = 7.9$x10^6$ assuming the flow to be fully turbulent. The result is that now the lift agrees well with that measured at 12° being only 0.007 too high, but the drag is 7.8 % too high. The results show not much improvement in the pressure distribution on the upper surface of the wing at section x/c = 0.3.

Another test case with α = 5°, Re = 7.9$x10^6$ was computed to see the agreement between the calculations and experiments in a situation where the vortex formation does not affect the result. In this case, the lift and drag coefficients agreed well with experimental results; the calculated lift coefficient is only 0.012 lower

and the drag coefficient is 0.2% lower than the corresponding measured value.

4.6 Vortex system

The vortex system can be visualized by the velocity vectors in a cross plane, as in Fig. 3. Both the measured and calculated results are drawn in the figure. As can be seen, the calculations compare favorably with the experiments in this case.

The distributions of the Reynolds stress component $-\overline{\rho v'w'}$ are depicted in Fig. 13 at cross-section $x/c = 0.3$ for $Re = 39x10^6$ and $\alpha=12^o$. The results obtained with the two different turbulence models differ considerably. However, the cross-flow velocities are relatively close to each other, as can be seen in Fig. 14.

For further analysis, the calculated and measured secondary separation lines on the upper surface can be compared for the case $Re = 19.8x10^6$ and $\alpha = 12^o$. For example, at $x/c = 0.37$, the secondary separation line is located at $y/s_{local} = 0.76$ in the calculations and at 0.74 in the experiments. In this respect, the agreement between the calculations and the experiments is very good.

5 Conclusions

The calculations past the ELAC-1 configuration using a Navier-Stokes flow solver with an advanced turbulence model EARSM produced only a modest Reynolds number dependence of the vortex structure and pressure distribution as opposed to the strong Reynolds number effect obtained in the corresponding experiments. This conclusion was obtained, although the transition and separation positions were varied in the calculations. However, at the lowest Reynolds number and at high angles of attack, the agreement between calculations and experiments was excellent, probably due to the right separation position. In addition, the agreement was again fairly good for the highest Reynolds number at a high angle of attack. Also, the vortex system was well captured at least qualitatively with primary, secondary and tertiary vortices.

The EARS turbulence model gave physically more correct results than the k-ω SST model.

Overall, it is concluded that the mechanism of the peculiarities observed in the experiments could not be fully clarified despite the considerable flow modeling effort.

Acknowledgements

References

[1] Neuwerth G, Peiter U, Decker F, and Jacob D. Reynolds Number Effects on the Low-Speed Aerodynamics of the Hypersonic Configuration ELAC-1. *AIAA 8th International Space Planes and Hypersonic Systems and Technologies Conference.* AIAA-98-1578, 1998.

[2] Krause E, Abstiens R, Fühling S, Vetlutsky V. Boundary-layer investigations on a model of the ELAC 1 configuration at high Reynolds numbers in the DNW. *Eur. J. Mech. B – Fluids* 19, pp. 745-764, 2000.

[3] Wallin S and Johansson A. An explicit algebraic Reynolds stress model for incompressible and compressible turbulent flows. *J. Fluid Mech.* 403, pp 89-132, 2000.

[4] Hämäläinen V. Implementing an Explicit Algebraic Reynolds Stress Model into the Three-Dimensional FINFLO Flow Solver. *Report B-52, Laboratory of Aerodynamics*, Helsinki University of Technology, 2001.

[5] Hellsten A. Some Improvements in Menter's *k*-ω SST Turbulence Model. *29th AIAA Fluid Dynamics Conference.* AIAA Paper 98-2554, 1998.

[6] Kaurinkoski P and Hellsten A. FINFLO: The Parallel Multi-Block Flow Solver. *Report A-17, Laboratory of Aerodynamics*, Helsinki University of Technology, 1998.
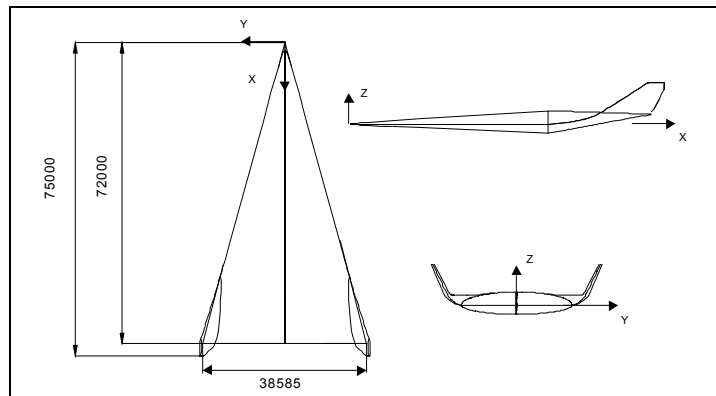
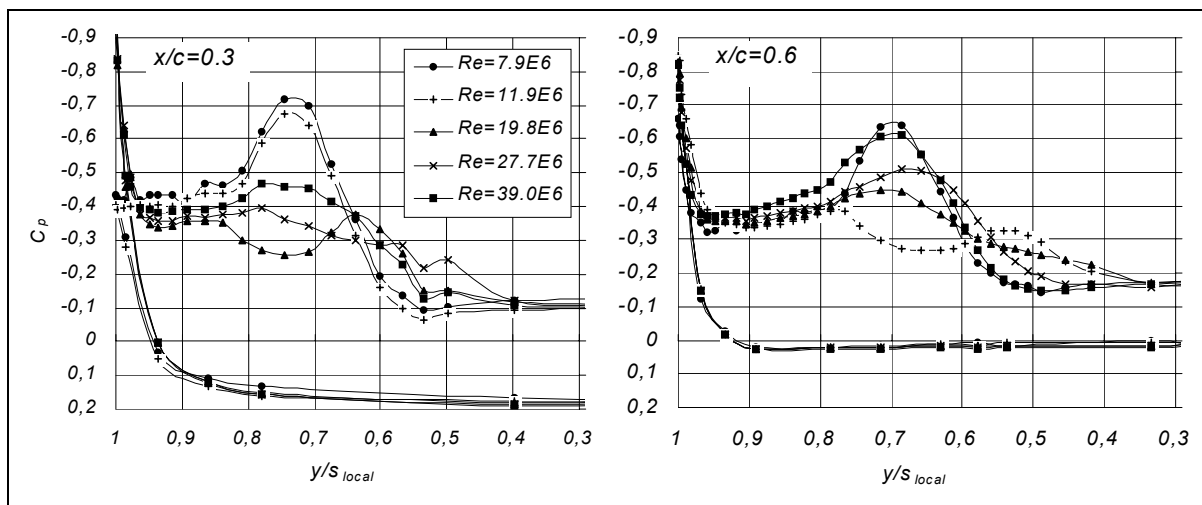Fig. 1 ELAC-1 configuration. Dimensions in mm.

Fig. 2 Measured pressure distributions on the upper surface of the wing at spanwise sections x/c=0.3 and x/c=0.6 at different Reynolds numbers at α=12°.
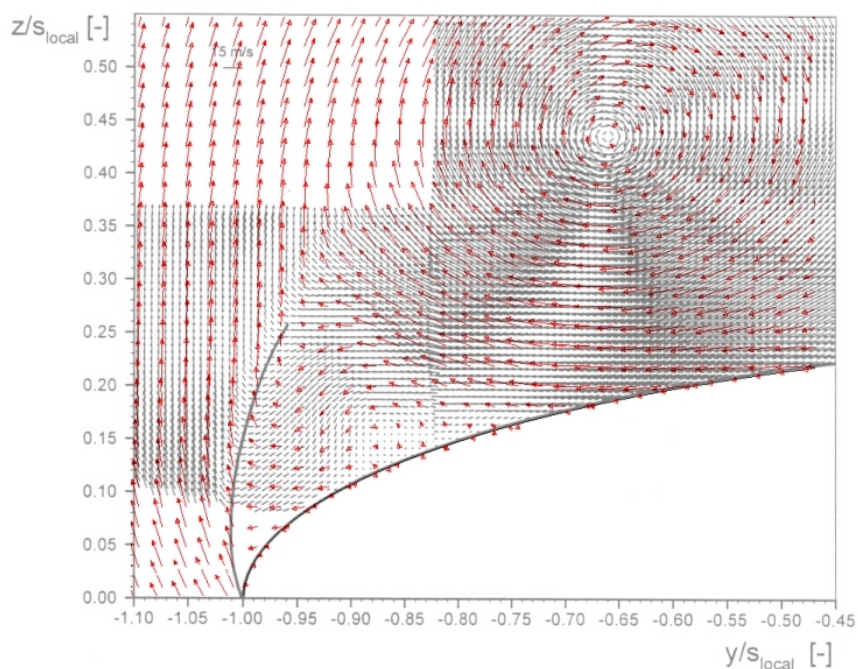

Fig. 3 Measured $\rightarrow$ and calculated $\rightarrow$ velocity vectors on a cross plane x/c=0.6 at Re=5.9x10^6, and at α=21°.

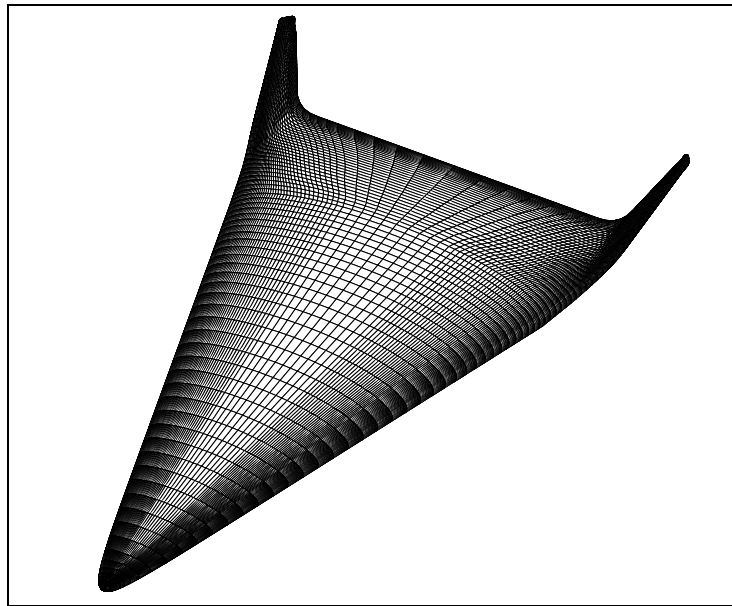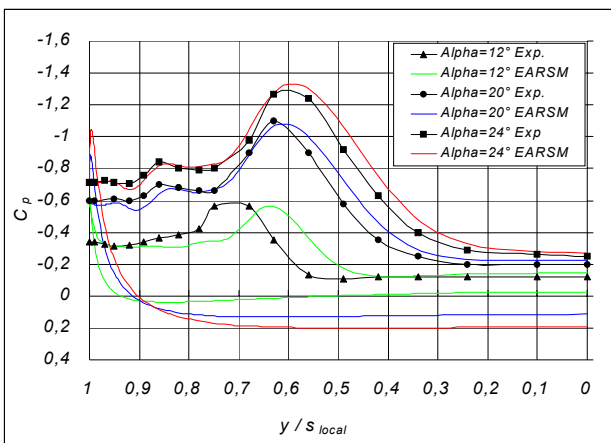Fig. 4 Surface grid duplicated for the full body. Only every second grid line shown.

Fig. 5 Calculated and measured pressure distributions on the surface of the wing at section x/c=0.6 at α =12°, 20° and 24° at Re=3.7x10^6.
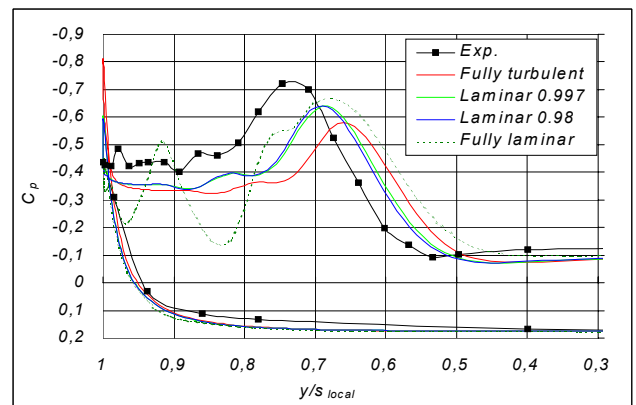
Fig. 7 Measured pressure distribution at section x/c=0.3 and calculated results assuming fully turbulent, fully laminar and partially laminar flow at Re=7.9x10^6.
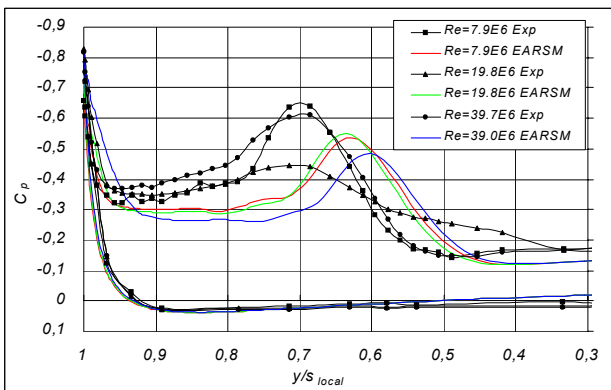
Fig. 6 Measured pressure distributions at x/c=0.6 and calculated results at x/c=0.6 assuming fully turbulent flow at α =12° and Re=7.9x10^6, 19.8x10^6, and 39x10^6.
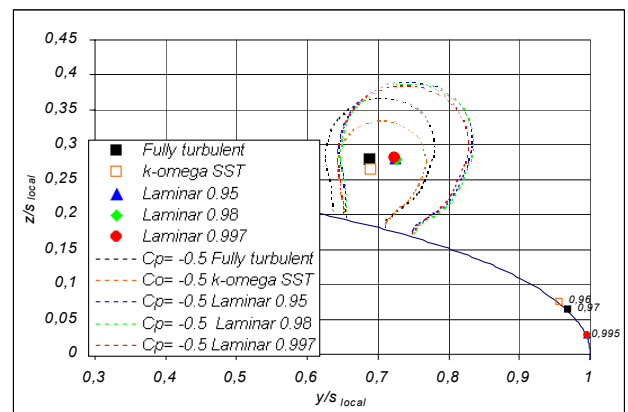
Fig. 8 Calculated separation and vortex axis positions and constant pressure coefficient line C_p=-0.5 for fully turbulent and for partially laminar boundary layers. α =12°, Re=7.9x10^6, x/c=0.3.
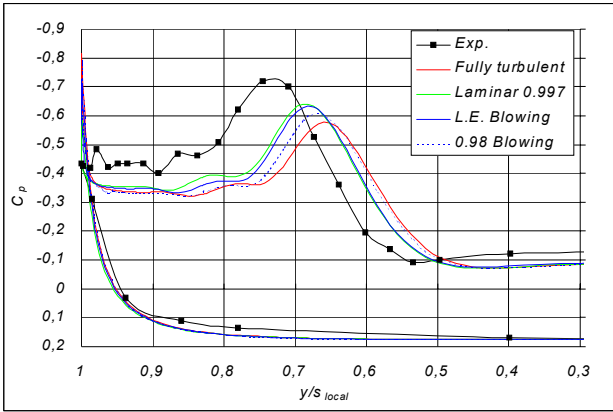
Fig. 9 Calculated pressure distributions on the surface of the wing at x/c=0.3 for fully turbulent cases without and with blowing and for partially laminar cases. Re=7.9x10^6.
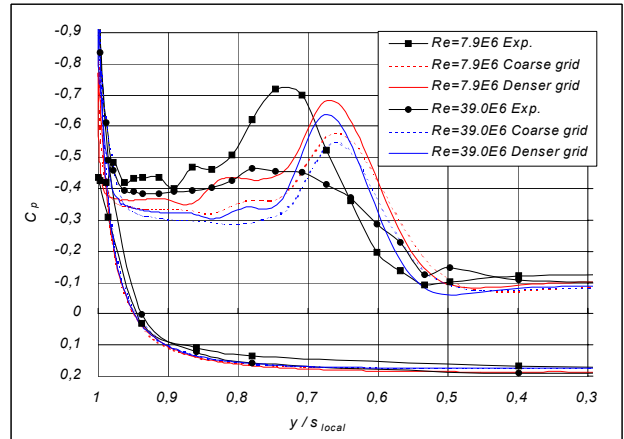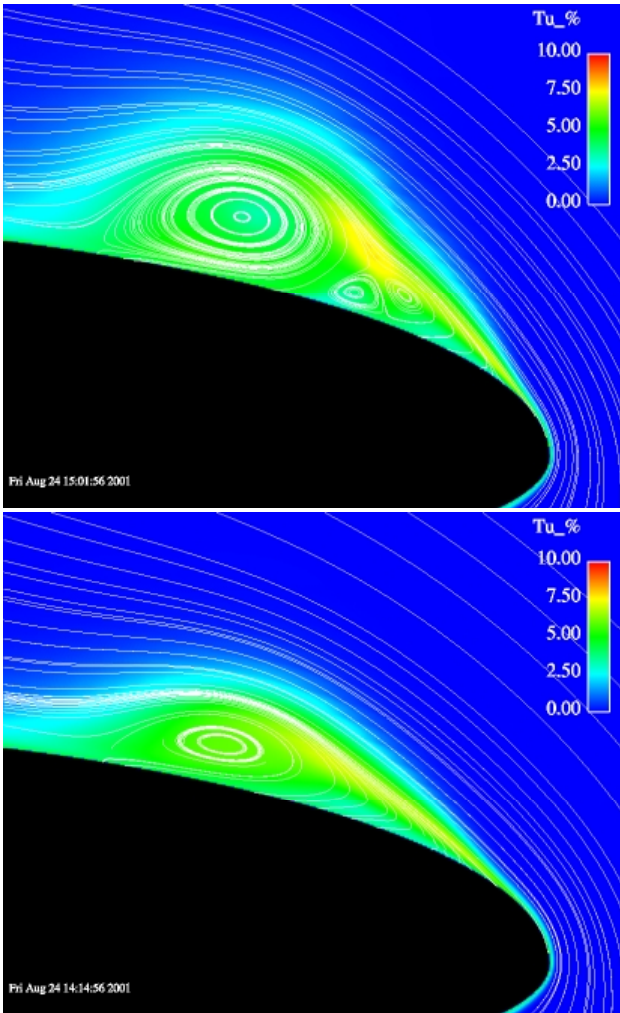

Fig. 10 Calculated flow field and intensity of turbulence at the cross-section x/c=0.3 at Re=39x10^6 using the EARS model (upper) and the k-ω SST model (lower).
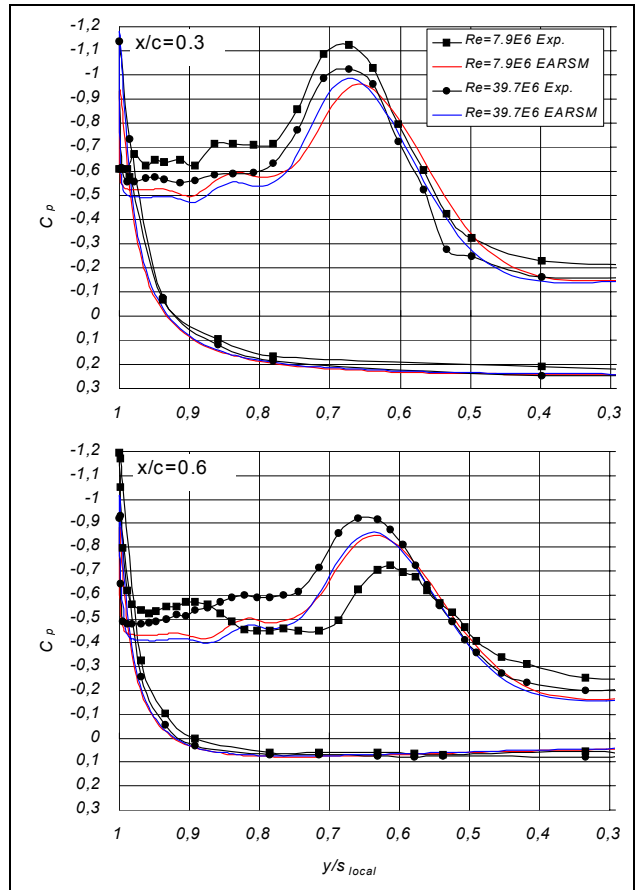

Fig. 11 Measured and calculated pressure distributions on the wing surface for the coarse grid and for the denser grid. x/c=0.3, α =12°.

Fig. 12 Calculated pressure distributions on the wing surface at x/c=0.3 and 0.6 at Re=7.9x10^6 and 39x10^6. α =16°.
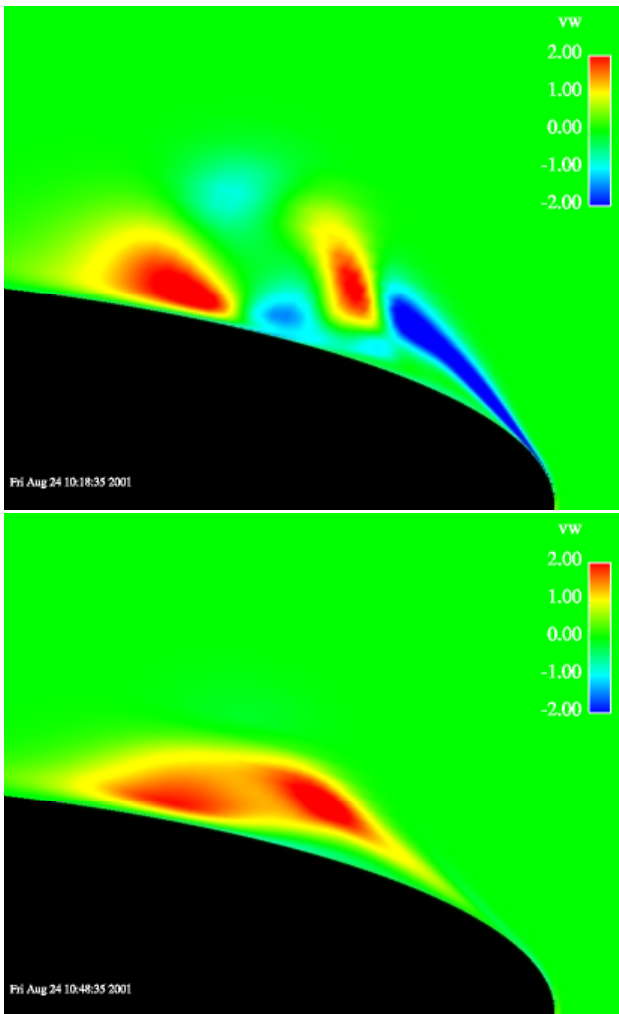
Fig. 13 Distribution of the Reynolds stress component $-\rho v'w'$ at x/c=0.3 for Re=39x10^6 and α=12$^\mathrm{o}$. Upper: EARS model, lower: k-ω SST model.
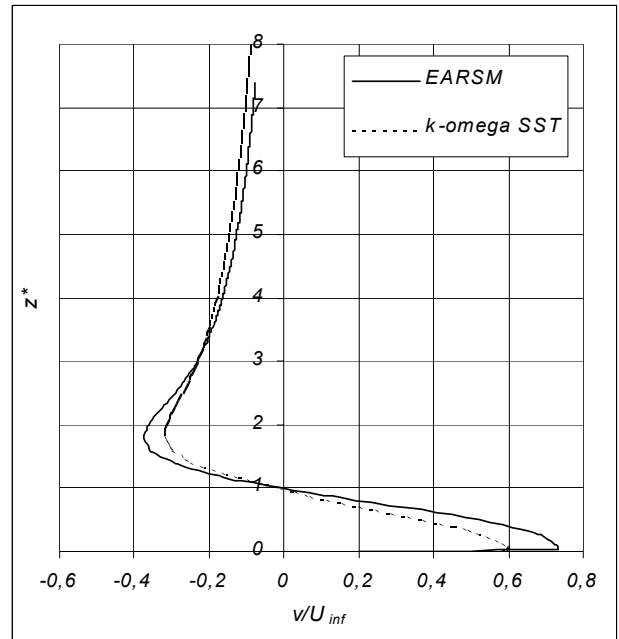

Fig. 14 Velocity component v in the y direction along a line through the axis of the primary vortex at x/c=0.3. Re=39x10^6 and α=12°.